An Optimization-Based Mesh-Generation Method for Image Representation

Seyedali Mostafavian and Michael D. Adams
Dept. of Electrical and Computer Engineering, University of Victoria
Victoria, BC, V8P 5C2, Canada
alimst@uvic.ca and mdadams@ece.uvic.ca

***Abstract*—In earlier work, Tu and Adams proposed the ERDED method, an effective technique for generating triangle-mesh models of digital images through explicit representation of discontinuities. In this paper, we propose a modified version of the ERDED method that generates a triangle mesh which better approximates the original image using an optimization-based algorithm. The proposed method is shown to produce image approximations of higher quality than those obtained by the ERDED method, both in terms of squared error and subjective quality. Moreover, this improvement in quality comes at a relatively modest computational cost, with the proposed method typically taking only a few seconds of computation time.**

I. Introduction

Images are most often represented by using a uniform sampling over a lattice. Uniform sampling, however, is almost never optimal because of selecting too many sample points in regions with small variations of the pixel intensity and too few sample points in regions with high changes of intensity. On the other hand, nonuniform sampling (i.e., sampling at a subset of points from a lattice) can choose sample points adaptive to the intensity variations in the image and is able to produce higher quality results with greater compactness and less memory cost, which is beneficial in many applications. This is why nonuniform sampling of images has received a considerable amount of attention from researchers recently [1]–[7].

Among the many models of image representations based on nonuniform sampling, triangle mesh models have become quite popular (e.g., [2]–[5], [8]–[13]). Triangle-mesh modeling of an image involves partitioning the image domain by a triangulation into a collection of non-overlapping triangles. The image function is then approximated over each triangle face. To represent an image using a mesh model, a method is needed to choose a good subset of sample points from the original image to generate such a mesh model. The method to generate the mesh model is known as a mesh-generation method. Often, approximating functions are chosen to be piecewise linear and continuous (e.g., [3], [5], [10], [11]). Images, however, usually contain a large number of discontinuities (i.e., image edges) and this leads to the fact that a mesh model that allows discontinuities in its approximating function may be beneficial as can be found in [1], [14], and [15].

In [1], Tu and Adams introduced a new mesh model for images, called ERD, which is based on constrained Delaunay triangulations (CDTs) [16] and an approximating function that explicitly represents image discontinuities. In this way, the approximating function allows for discontinuities across constrained edges in the triangulation. In order to obtain an ERD mesh model, two mesh-generation methods were proposed in [1] of which the one using the error-diffusion (ED) technique from [5] is called the ERDED mesh-generation method. Although quite effective, the ERDED method has the weakness that it often chooses suboptimal parameters for the model, leading to a degradation in approximation quality. This problem, as will be seen later, is even worse when modeling less-sharp image edges. In this paper, we propose a modified version of the ERDED method that utilizes an optimization-based algorithm for selecting the parameters of the model to minimize the approximation error. Through experimental results, we show that our proposed method yields image approximations of higher quality (i.e., with lower squared error) than the ERDED method, with a relatively modest computational cost.

The remainder of this paper is organized as follows. Section II provides some background information on triangle-mesh models for image representation and introduces basic concepts of the ERD mesh model and the ERDED mesh-generation method essential to the understanding of this paper. Our proposed mesh-generation method is presented in Section III. This is done by describing the weakness of the ERDED method in choosing the model parameters, and explaining how they are optimized in our proposed method to minimize the approximation error. Through experimental results, Section IV shows that our proposed method yields image approximations of higher quality than the ERDED method, in terms of squared error and subjective quality, with a relatively modest computational cost. Finally, Section V concludes with a summary of our work.

II. Background

In what follows, the cardinality of a set S is denoted by $|S|$. Consider an image function ϕ defined on a truncated (2-dimensional) integer lattice Λ of width W and height H. A triangle mesh model of ϕ consists of: 1) a set $P = \{p_i\} \subset \Lambda$ of sample points and their corresponding function values $\{z_i = \phi(p_i)\}$; and 2) a triangulation T of P. As a matter of terminology, the size and sampling density of the model are defined as $|P|$ and $|P|/|\Lambda|$, respectively. The mesh model is associated with a piecewise-linear approximating function $\hat{\phi}$ that interpolates ϕ at each point in P. In other words, over each face in T, $\hat{\phi}$ specifies a unique linear function that interpolates ϕ at the three vertices of the face. In our work, the quality of a

978-1-4673-7788-1/15/$31.00 ©2015 IEEE

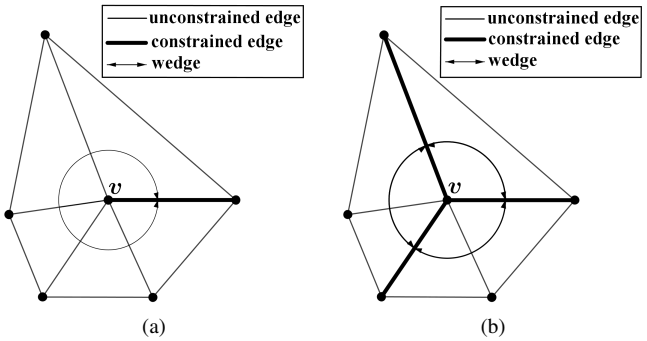

(a) (b)

Fig. 1: The relationship between vertices, constrained edges, and wedges. The (a) single-wedge and (b) multiple-wedge cases.

mesh is evaluated by the mean squared error (MSE) ϵ between $\hat{\phi}$ and ϕ, where

$$\epsilon = \frac{1}{|\Lambda|} \sum_{p \in \Lambda} \left(\hat{\phi}(p) - \phi(p) \right)^2 .$$

The MSE is typically expressed in terms of the peak signal-to-noise ratio (PSNR), which is defined as $\mathsf{PSNR} = 20 \log_{10} [(2^\rho - 1)/(\sqrt{\epsilon})]$, where ρ is the number of bits per sample in the image ϕ. The PSNR is usually represented using a decibel (dB) scale, with greater PSNR corresponding to lower MSE and higher quality reconstructed images.

ERD Model. Since our work uses the ERD mesh model introduced in [1], it is worthwhile to make a few brief comments about this model here. As mentioned earlier, the ERD model is based on the CDT and allows the piecewise-linear approximating function to be discontinuous across the constrained edges in the triangulation. In the ERD model, constrained edges are used to represent the image edges. A set of consecutive triangle faces in a loop around a vertex $v \in P$ that are not separated by any constrained edge is called a *wedge*. This definition is illustrated in Fig. 1. Each wedge of a vertex has associated with it what is called a *wedge value*. The wedge value z of the wedge w belonging to vertex v specifies the limit of $\hat{\phi}(p)$ as p approaches v from points inside the wedge w. Then, over each triangle face f in the triangulation, $\hat{\phi}$ defines a unique linear function that interpolates the three wedge values of f corresponding to its three vertices. The wedge values in the ERD model, as will be explained later, are the parameters of interest in this paper.

ERDED Method. As mentioned earlier, one of the effective methods proposed in [1] for generating the ERD mesh models of images is the ERDED mesh-generation method. Since our proposed method builds on the ERDED method, we briefly describe this method here. The ERDED method selects the parameters of the ERD model (i.e., a set P of sample points, a set E of constrained edges, and wedge values) to obtain the best possible approximation $\hat{\phi}$ of the original image ϕ for a specific target number N of sample points. The general algorithmic framework of the ERDED mesh-generation method consists of the following steps:

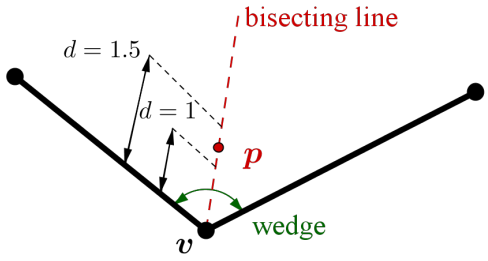

Fig. 2: The line search process used in the ERDED method for selecting wedge values.

1) *Initial triangulation.* Select initial values for P and E. This is performed using a modified Canny edge detector followed by a polyline approximation of the detected edges. Then, construct a CDT of P with edge constraints E. Let $N_0 = |P|$ be the initial mesh size.
2) *Initial wedge values.* Calculate the wedge value for each wedge w of each vertex $v \in P$.
3) *Point Selection.* Select a new sample point q to add to the mesh. The set of new sample points S (where, $|S| = N - N_0$) is chosen using the error-diffusion technique from the ED method in [5].
4) *Point insertion.* Insert the point q in the triangulation. If q is on a constrained edge, split the edge at q into two constrained edges, and compute the wedge value for each new wedge of the vertex q. (If q is not on a constrained edge, the wedges and wedge values remain the same and no special action is required.)
5) *Stopping criterion.* If $|P| < N$, go to step 3.

Wedge-Value Calculation. Since our work mainly focuses on improving step 2 in the framework above, we describe how wedge values are calculated in step 2 in more detail. Consider a CDT of P with edge constraints E. If only one wedge is associated with the vertex $v \in P$, the corresponding wedge value z is simply chosen as the value of the image function at vertex v (i.e., $z = \phi(v)$). Otherwise, if two or more wedges are associated with the vertex v, the wedge value z associated with each wedge is chosen using a line search as follows. The grid points along the ray originating from v and bisecting the wedge are searched. During the line search, the point p, at which the maximum magnitude second-order directional derivative (MMSODD) is largest, is selected as shown in Fig. 2. Then, the wedge value z is chosen as the value of the image at p (i.e., $z = \phi(p)$). To prevent p from falling far outside of the corresponding face, the line search is restricted to distance $d \in [1, 1.5]$ units from v as shown in Fig. 2. The obtained wedge value is then rounded to the nearest integer value.

III. Proposed Mesh-Generation Method

Having introduced the necessary background, we now turn our attention to introducing the mesh-generation method proposed in this paper. As mentioned previously, our method is essentially a modified version of the ERDED scheme. The ERDED method, as explained earlier, employs a restricted local line search to choose the wedge values required by the ERD model. In what follows, first, we consider two different image-edge profiles and analyze how the restricted local line

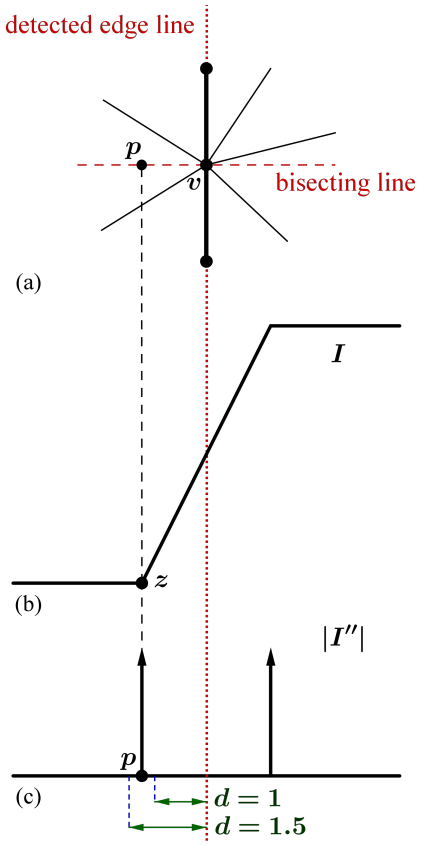

Fig. 3: Sharp image-edge profile. The (a) top view of the triangulation, (b) cross-section of the image intensity, and (c) magnitude of the second-order directional derivative of the image intensity.

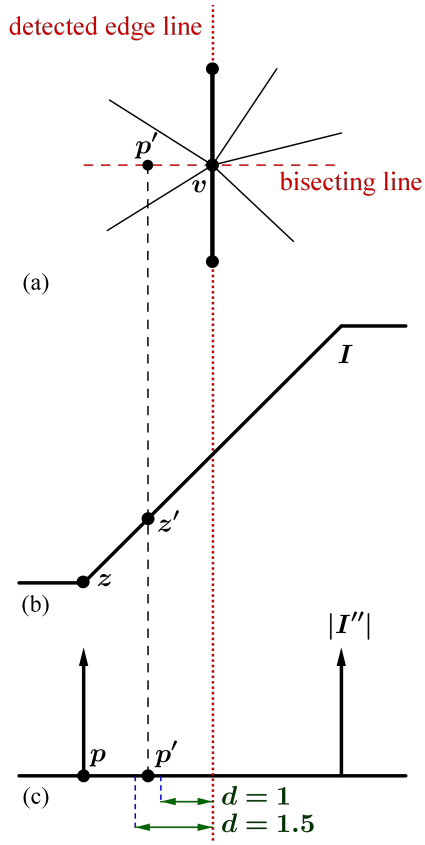

Fig. 4: Less-sharp image-edge profile. The (a) top view of the triangulation, (b) cross-section of the image intensity, and (c) magnitude of the second-order directional derivative of the image intensity.

search of the ERDED method performs for each profile. One profile is the case where the restricted local line search selects the wedge values properly, and the other one, which commonly happens in images, is the case where the restricted local line search fails to select the correct wedge values. Then, we present our proposed algorithm to overcome this problem, leading to the proposed mesh-generation method.

Figs. 3 and 4 show sharp and less-sharp image-edge profiles, respectively, including the corresponding part of the triangulation, the image intensity function I, and the magnitude of its second-order directional derivative $|I''|$. For the sake of illustration, a simple ramp function with a relatively steep slope is used in Fig. 3(b) to represent the image intensity across a sharp edge in the image; and a ramp function with a gentle slope is used in Fig. 4(b) to represent the image intensity across a less-sharp edge. The thicker edges in Figs. 3(a) and 4(a) correspond to the constrained edges in the triangulation, representing the image edges. The dotted line passing through the middle of each edge profile corresponds to the image edges detected by the edge detector. Therefore, two wedges are formed, one on each side of the constrained edges and incident to vertex v in Figs. 3(a) and 4(a). In this analysis, we only consider the process of calculating the wedge value of the wedge on the left side of the constrained edges. A similar analysis applies to the wedge on the other side.

As explained earlier, the local line search of the ERDED method tries to find the point with the highest MMSODD along the bisecting line. In the case of the sharp-edge profile shown in Fig. 3, the point with the highest MMSODD, which is denoted by p in Figs. 3(a) and 3(c), falls inside the fixed distance range of the line search (i.e., between $d = 1$ and $d = 1.5$) as can be seen in Fig. 3(c). Thus, the point p is correctly detected during the line search. Then, the intensity value z at the point p is selected from Fig. 3(b) as the wedge value associated with the wedge on the left side of the constrained edges.

In contrast, in the case of a less-sharp edge profile shown in Fig. 4, the desired point p with highest MMSODD is not guaranteed to fall inside the fixed search range of $d \in [1, 1.5]$. As displayed in Fig. 4(c), the line search fails to detect the point p. Instead, another point p' within the range of $d \in [1, 1.5]$ is selected. Consequently, instead of the correct intensity value z at p, the improper intensity value z' at p' is selected from Fig. 4(b) as the wedge value of the wedge on the left side of the constrained edges.

Since an image contains different edge profiles with various sharpness levels, no single fixed range of line search can be found that works best for all edge profiles. This problem of the line search leads to suboptimal wedge values in the case of less-sharp edges in the image, resulting in a degradation in

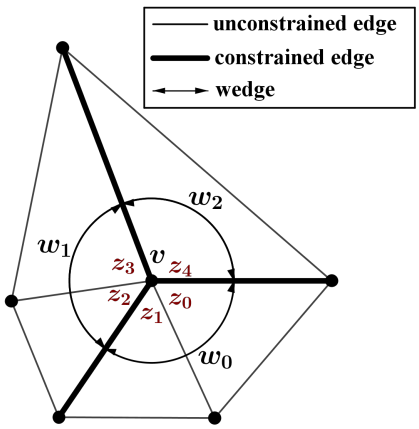

Fig. 5: The relationship between wedges, corners, and corner z values.

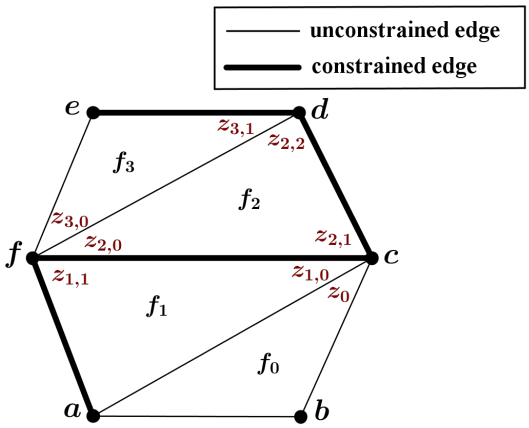

Fig. 6: An example of a triangulation showing the corner z values to be optimized.

approximation quality inside the wedge of interest.

The analysis mentioned above motivated us to employ a more accurate approach to find the best possible wedge values, which are used to construct the approximating function over the faces. The proposed scheme exploits an optimization-based algorithm to find the wedge values instead of using a local line search. Before introducing the proposed algorithm, the term *corner z value* should be defined. Recall from Fig. 1 that a wedge is a set of triangles surrounded by two constrained edges incident on a vertex. Thus, a wedge incident on a vertex contains one or more triangle corners. Each triangle corner inside a wedge is associated with a value, which is called a *corner z value*.

Fig. 5 shows an example of a triangulation with three constrained edges incident to the vertex v. As can be seen in Fig. 5, the triangulation consists of three wedges denoted by w_0, w_1, and w_2. The wedge w_0 contains two corners associated with the corner z values z_0 and z_1. Similarly, the wedge w_1 contains two corners associated with the corner z values z_2 and z_3, but the wedge w_2 only contains one corner associated with the corner z value z_4. Similar to wedge values, the corner z value of a triangle corner incident to a vertex v specifies the limit of the approximating function $\hat{\phi}$ at the point p as p approaches v from points inside the triangle.

Having introduced the corner z values, we now describe the proposed optimization-based algorithm for selecting the wedge values. For each triangle f in the triangulation, the corner z values $\{z_i\}_{i=0}^{2}$ associated with the corners of f are optimized to minimize the total (pixelwise) squared error between the linear approximating function $\hat{\phi}$ and the original image function ϕ over f. The optimization problem introduced above is given by

$$\underset{\{z_i\}}{\text{minimize}} \sum_{p\in\Omega} \left|\hat{\phi}(p) - \phi(p)\right|^2, \tag{1}$$

where Ω is the set of grid points in the face f. The minimization problem (1) is a typical least-squares problem, which can be efficiently solved by linear methods. In (1), the only z values of the corners that are considered for optimization are those associated with a vertex incident to more than one constrained edge. In the case of a vertex incident to zero or one constrained edge, the corresponding corner z values are simply set to the values of the original image at the corresponding sample points.

Fig. 6 illustrates an example of a triangulation with four faces f_0 to f_3. As can be seen in Fig. 6, only z values of the corners incident to the vertices c, d, and f are considered for optimization. Thus, only the corner z value z_0 is optimized for the face f_0. Similarly, only the two corner z values $z_{1,0}$ and $z_{1,1}$ for f_1, and $z_{3,0}$ and $z_{3,1}$ for f_3 are optimized. Finally, for f_2, all three corner z values $z_{2,0}$, $z_{2,1}$, and $z_{2,2}$ are considered for optimization. The z values of the corners associated with vertices a, b, and e interpolate the original values at sample points a, b, and e, respectively.

The optimization-based method described above yields different corner z values inside the same wedge, introducing discontinuities along the unconstrained edges inside the wedge. In the ERD model, however, discontinuities are only allowed across the constrained edges. So, for the mesh to properly model the discontinuities, all corners inside the same wedge should have the same z value (same as wedge value in ERD model). To accomplish this, the wedge value of each wedge is obtained by averaging all corner z values inside the same wedge. The wedge value is then rounded to the nearest integer value. This procedure gives us a modified ERDED mesh-generation method that uses the proposed optimization-based algorithm for selecting the wedge values instead of the local line search.

IV. Results

Having introduced our proposed method, the modified ERDED, we now evaluate its performance by comparing it in terms of mesh quality with the ERDED method. For test data, in this paper, we focus our attention on the set of five images listed in Table I, which were deliberately chosen to include photographic, medical, and computer-generated imagery. To evaluate the performance of our proposed mesh-generation method, we proceeded as follows. For each of our five test images, we used each of the proposed and ERDED methods

TABLE I: Test images

Image	Size, Bits/Sample	Description
peppers	512×512, 8	collection of peppers [17]
lena	512×512, 8	woman [17]
ct	512×512, 12	CT scan of head [18]
bull	1024×768, 8	computer-generated bull [19]
wheel	512×512, 8	computer-generated wheel

to generate a mesh with four sampling densities. Then, for each method, the mean-squared error between the original image and the reconstructed image was measured in terms of PSNR. Table II shows the results for the five images listed in Table I. In Table II, the best result in each test case is highlighted in bold. The sampling densities for which results are presented are chosen to be representative of the range that would typically be used for each image in practice (which differs from image to image). From Table II, we can see that our proposed method outperforms the ERDED scheme in 18/20 of the test cases by a margin of up to 5.06 dB. From these results, it is clear that our proposed method is able to produce meshes of higher quality, in terms of PSNR, than the ERDED method.

In the above evaluation, PSNR was found to correlate reasonably well with subjective quality. For the benefit of the reader, however, we provide a visual example. In order to show the location and intensity of the approximation error for a reconstructed image, an *error image* is used. An error image is obtained simply by taking the absolute difference between the original image and the reconstructed image pixelwise. Then, the difference image is inverted for better visualization. Thus, in the error image, darker pixels correspond to pixels with higher approximation error. For one of the test cases from Table II (i.e., the bull image at a sampling density of 0.25%), Fig. 7 shows an example of an area in the image where the proposed method produces results with lower approximation error compared to the ERDED method. The triangulation shown in Fig. 7(c) is the same for both the proposed and ERDED methods. As can be seen in the error images shown in Figs. 7(d) and (e), the proposed method, which uses the optimization-based algorithm for calculating the wedge values, is able to produce results with lower error than the ERDED method, which uses a local line search. Similarly, another example from the lena image at a sampling density of 1% is illustrated in Fig. 8. As can be seen in the error images shown in Figs. 8(d) and (e), the proposed optimization-based method leads to lower approximation error than the ERDED method in the area of the interest. The better performance in the case of the proposed method is entirely because of the fact that the wedge values, which are employed by the approximation function over each triangle face, are obtained using the optimized corner z values as explained in Section III. Consequently, the problem associated with the local line search described previously in Fig. 4 is avoided through the proposed optimization-based scheme.

In terms of complexity, our proposed method has a relatively low computational cost. In our work, the optimization problem is solved using the well-known steepest-descent method (Section 6.9 in [20]) and it only increases the total execution time by a few seconds on a modest computer with a 3 GHz Intel Core 2 Duo CPU. For example, to generate a mesh for the lena image with a sampling density of 2%, the proposed method takes less than 3 seconds. So, the use of the proposed optimization-based algorithm for selecting the wedge values does not result in a complicated and slow mesh-generation scheme requiring execution times on the order of minutes.

TABLE II: Comparison of the mesh quality obtained with the proposed and ERDED methods

Image	Sampling Density (%)	PSNR(dB)	
		Proposed	ERDED
peppers	0.5	**22.49**	22.14
	1	**26.47**	25.97
	2	**29.26**	29.00
	3	**30.37**	30.17
lena	0.5	**20.81**	20.55
	1	**26.14**	25.81
	2	**29.38**	29.28
	3	31.30	**31.31**
ct	0.125	**18.72**	15.63
	0.25	**27.42**	25.97
	0.5	**31.62**	30.06
	1	**36.62**	36.51
bull	0.125	**25.22**	24.68
	0.25	**29.47**	28.86
	0.5	**35.35**	35.15
	1	**39.21**	39.02
wheel	0.0625	**35.75**	30.69
	0.125	**36.54**	34.55
	0.25	**37.24**	35.56
	0.5	37.38	**37.86**

V. Conclusions

In this paper, we proposed an improved technique for generating ERD mesh models of images, based on the ERDED scheme. Our proposed method employs an optimization algorithm to better exploit the image content and to reduce the approximation error in the reconstructed image. Through experimental results, our proposed method was shown to produce image approximations of higher quality than those obtained with the ERDED scheme, both in terms of PSNR and subjective quality. The improved approximation quality produced by our method comes at a relatively modest computational cost. Therefore, our proposed method is of potential benefit to many image processing and computer graphics applications that employ mesh models of images.

References

[1] X. Tu and M. Adams, "Improved mesh models of images through the explicit representation of discontinuities," *Electrical and Computer Engineering, Canadian Journal of*, vol. 36, pp. 78–86, Spring 2013.

[2] M. Adams, "A flexible content-adaptive mesh-generation strategy for image representation," *Image Processing, IEEE Transactions on*, vol. 20, pp. 2414–2427, Sept 2011.

[3] R. Verma, G. Srivastava, R. Mahrishi, and S. Rajesh, "A fast image reconstruction algorithm using significant sample point selection and linear bivariate splines," in *IEEE Region 10 Conference*, pp. 1–6, Jan 2009.

[4] M. Grundland, C. Gibbs, and N. A. Dogson, "Stylized multiresolution image representation," *Journal of Electronic Imaging*, vol. 17, no. 1, pp. 013009.1–17, 2008.

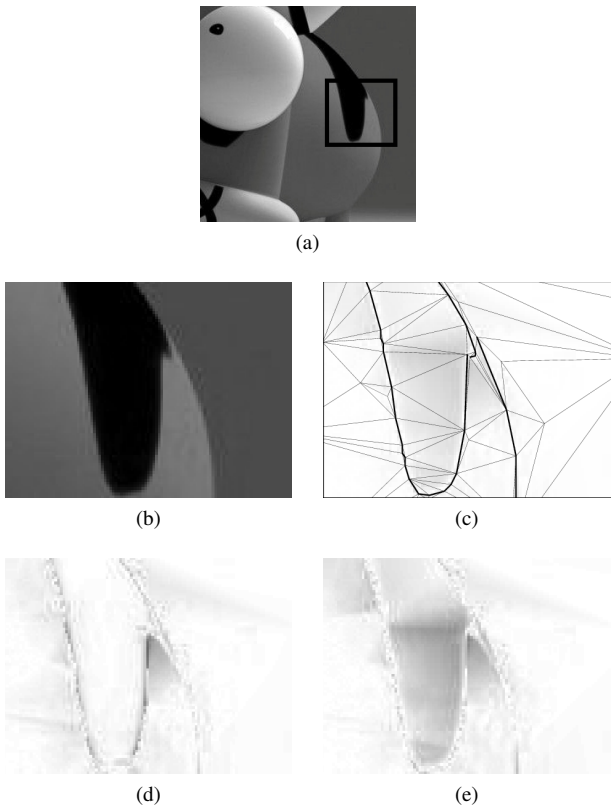

(a) (b) (c) (d) (e)

Fig. 7: Visual comparison of approximation errors obtained by the proposed and ERDED methods for the bull image at a sampling density of 0.25%. (a) Part of bull image with region of interest marked with black rectangle. (b) The magnified area of interest. (c) Corresponding triangulation with constrained edges as thick lines. (d) and (e) The error images from the proposed and ERDED methods, respectively.

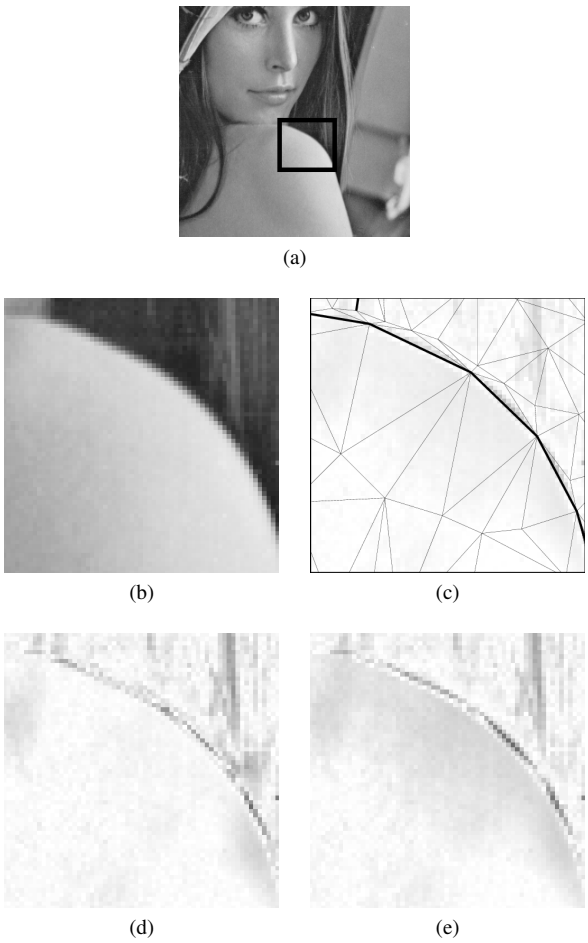

(a) (b) (c) (d) (e)

Fig. 8: Visual comparison of approximation errors obtained by the proposed and ERDED methods for the lena image at a sampling density of 1%. (a) Part of lena image with region of interest marked with black rectangle. (b) The magnified area of interest. (c) Corresponding triangulation with constrained edges as thick lines. (d) and (e) The error images from the proposed and ERDED methods, respectively.

[5] Y. Yang, M. Wernick, and J. Brankov, "A fast approach for accurate content-adaptive mesh generation," *Image Processing, IEEE Transactions on*, vol. 12, pp. 866–881, Aug 2003.

[6] X. Shen, G. Zeng, and Z. Wei, "Nonuniform sampling and reconstruction for high resolution satellite images," in *Image Analysis and Signal Processing (IASP), International Conference on*, pp. 187–191, Oct 2011.

[7] M. Sarkis and K. Diepold, "Content adaptive mesh representation of images using binary space partitions," *Image Processing, IEEE Transactions on*, vol. 18, pp. 1069–1079, May 2009.

[8] H. Zhou, J. Zheng, and L. Wei, "Representing images using curvilinear feature driven subdivision surfaces," *Image Processing, IEEE Transactions on*, vol. 23, pp. 3268–3280, Aug 2014.

[9] L. Demaret and A. Iske, "Adaptive image approximation by linear splines over locally optimal delaunay triangulations," *Signal Processing Letters, IEEE*, vol. 13, pp. 281–284, May 2006.

[10] A. Sanchez-Beato and G. Pajares, "Noniterative interpolation-based super-resolution minimizing aliasing in the reconstructed image," *Image Processing, IEEE Transactions on*, vol. 17, pp. 1817–1826, Oct 2008.

[11] M. Sarkis and K. Diepold, "A fast solution to the approximation of 3d scattered point data from stereo images using triangular meshes," in *Humanoid Robots, 7th IEEE-RAS International Conference on*, pp. 235–241, Nov 2007.

[12] J. Brankov, Y. Yang, and M. Wernick, "Tomographic image reconstruction based on a content-adaptive mesh model," *Medical Imaging, IEEE Transactions on*, vol. 23, pp. 202–212, Feb 2004.

[13] P. iviciolu and M. Al, "Impulsive noise suppression from highly distorted images with triangular interpolants," *International Journal of Electronics and Communications*, vol. 58, no. 5, pp. 311 – 318, 2004.

[14] T. Xia, B. Liao, and Y. Yu, "Patch-based image vectorization with automatic curvilinear feature alignment," *ACM Trans. Graph.*, vol. 28, pp. 115:1–115:10, Dec. 2009.

[15] M. Hugentobler and B. Schneider, "Breaklines in coons surfaces over triangles for the use in terrain modelling," *Computers and Geosciences*, vol. 31, no. 1, pp. 45 – 54, 2005.

[16] L. P. Chew, "Constrained delaunay triangulations," in *Proceedings of the Third Annual Symposium on Computational Geometry*, SCG '87, pp. 215–222, ACM, 1987.

[17] USC-SIPI database. Available at: http://sipi.usc.edu/database, 2014.

[18] JPEG-2000 test images. ISO/IEC JTC 1/SC 29/WG 1N 545, July 1997.

[19] Michael Adams' research datasets. Available at: http://www.ece.uvic.ca/ mdadams/datasets, 2011.

[20] S. Rao, *Engineering Optimization: Theory and Practice*. Wiley, 4 ed., 2008.